Thermally Activated Delayed Fluorescence in a Mechanically Soft Charge-Transfer Complex: Role of the Locally Excited State

Kalyan Jyoti Kalita, Saikat Mondal, C. Malla Reddy,[*] and Ratheesh K. Vijayaraghavan[*]

Department of Chemical Sciences

Indian Institute of Science Education and Research Kolkata

Mohanpur, Nadia, West Bengal, 741246, India

E-mail: cmreddy@iiserkol.ac.in, ratheesh@iiserkol.ac.in

Table of Contents:

Experimental Methods and Materials

Materials: All the precursor materials and acceptor molecules used are procured from Sigma-Aldrich and used after recrystallisation. All solvents were purchased from Sigma-Aldrich. Solvents were dried or distilled before use by standard laboratory purification techniques. TLC analysis was performed on recoated Aluminium plates of silica gel 60 F254 plates (0.25 mm, Merck).

NMR Measurements: NMR spectra were collected using a BRUKER (^{1}H: 500 MHz) instrument.

Elemental Analysis: Elemental analysis was performed on a PerkinElmer CHN Analyser (Series II 2400 series).

IR Analysis: FT-IR spectra were recorded on a PerkinElmer FT-IR instrument (model No: PerkinElmer FT-IR Spectrum Two).

FE-SEM: Field emission scanning electron microscopy (FE-SEM) images were recorded in a ZEISS (model no: DSM 950) instrument. The samples were gold-coated, and the micrographs were taken using a scanning electron microscope (Zeiss DSM 950).

Differential scanning calorimetry: DSC thermogram was recorded on a PerkinElmer instrument (DSC 4000) for melting point analysis.

Thermo gravimetric analysis: TGA thermogram was recorded on a PerkinElmer instrument (model no: PerkinElmer Thermogravimetric Analyzer TGA 4000).

HPLC Measurements: HPLC was recorded on a Waters HPLC instrument with a Photodiode Array Detector using an Agilent C-18 column (150 × 4.6 mm).

HRMS Measurements: HRMS was recorded on a Waters HRMS instrument (model no: Waters XEVO G2-XS QTOF).

Electron paramagnetic resonance measurements: EPR spectra were recorded on a Bruker spectrometer (Model No: Bruker, EMXmicro) at room temperature.

Single crystal X-ray diffraction (SCXRD): SCXRD data were collected at 100 K (low temperature) and 293K (room temperature) on a Rigaku (dual, Cu/Mo at zero Eos) diffractometer using monochromatic Cu-Kα radiation having a 100 μm beam size. The structure was solved by Olex2 (1.2.9 version) with the SHELXT structure solution program *via* an intrinsic phasing algorithm. The ShelXL refinement package using least square minimisation was utilised to refine the structure.[1-2] Displacement parameters of all non-hydrogen atoms were refined anisotropically. Mercury (3.10.1 version) software was used to prepare all the crystal packing diagrams.

PXRD specifications: The PXRD pattern was collected on a Rigaku Mini Flex with Cu Kα radiation (1.540 Å). The tube voltage and amperage were set at 40 kV and 15 mA, respectively. The instrument was previously calibrated using a silicon standard.

Nanoindentation: We performed the nanoindentation experiments on (010) and (100) faces of ETC-TFDCNB crystals. Face indices were identified from SCXRD. Crystals were mounted using Fevi kwik glue on a stainless-steel disk-shaped sample holder with a smooth surface. The experiments were carried out using a nanoindenter (Hysitron Triboindenter, TI Premier, Minneapolis, USA) with a three-sided pyramidal Berkovich diamond indenter tip of radius 150 nm having an in-situ Scanning Probe Microscopy (SPM) facility. Before nanoindentation, the tip area function was calculated from a series of indentations on a standard fused quartz sample. The indentations were performed under the load control mode, fixing the peak load (P_{max}) at 5 mN. The obtained $P–h$ curves were analysed using the standard Oliver–Pharr method to extract the crystals' elastic modulus (E) and hardness (H).[3]

Optical Measurements: Electronic absorption spectra were recorded on a PerkinElmer UV-Vis-NIR spectrometer using a quartz cuvette (1 cm path length) for the solution state and a 2.5 cm x 2.5 cm quartz plate for the thin film state. Photoluminescence emission (PL) spectra were recorded on EDINBURGH-FLS1000 spectrometers using appropriate correction files. PL spectra of solid-state (film/crystal) were recorded in a front-face geometry. Temperature-dependent PL experiment of the samples in solid-state is performed in EDINBURGH-FLS1000 with the cryostat (Oxford Instruments Optistat DN model) setup using liquid nitrogen as a cryogen. The Time correlated single photon counting (TCSPC) measurements were recorded using a Horiba Delta flex-01 TCSPC spectrometer. Time-correlated single-photon counting (TCSPC) data were collected using Horiba Delta Flex-01-DD, coupled with 405 nm, 450 nm and 532 nm diode laser for excitation. SpectraLED of 415 nm and 461 nm as an excitation source was used to obtain the long-lived components in the micro-second region in the same instrument. Instrument response function (IRF) was collected using a colloidal dispersion of Ludox. Horiba EzTime software was used to fit the transient decay curves. The decay curves were best fitted by considering the fitting parameter (χ^2) and after a visual inspection of the residuals. Absolute photoluminescence quantum yields were measured using an integrating sphere accessory with the same instrument. The solid crystalline sample was used for PLQY measurements.

Optical images and videos: The optical images and videos of mechanical deformation were taken using a Leica microscope.

Strength of donor (D) and acceptor (A) unit considered in this study: The extent of charge transfer (CT) interaction depends on the HOMO level of D and LUMO level of the A unit.

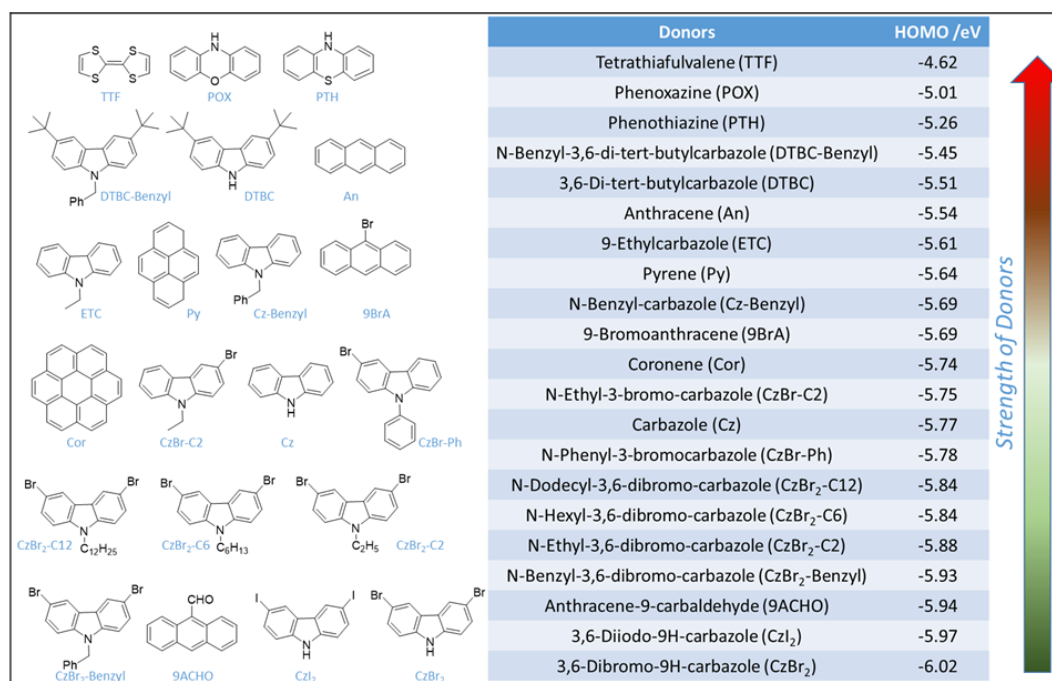| Donors	HOMO /eV
Tetrathiafulvalene (TTF)	-4.62
Phenoxazine (POX)	-5.01
Phenothiazine (PTH)	-5.26
N-Benzyl-3,6-di-tert-butylcarbazole (DTBC-Benzyl)	-5.45
3,6-Di-tert-butylcarbazole (DTBC)	-5.51
Anthracene (An)	-5.54
9-Ethylcarbazole (ETC)	-5.61
Pyrene (Py)	-5.64
N-Benzyl-carbazole (Cz-Benzyl)	-5.69
9-Bromoanthracene (9BrA)	-5.69
Coronene (Cor)	-5.74
N-Ethyl-3-bromo-carbazole (CzBr-C2)	-5.75
Carbazole (Cz)	-5.77
N-Phenyl-3-bromocarbazole (CzBr-Ph)	-5.78
N-Dodecyl-3,6-dibromo-carbazole (CzBr$_2$-C12)	-5.84
N-Hexyl-3,6-dibromo-carbazole (CzBr$_2$-C6)	-5.84
N-Ethyl-3,6-dibromo-carbazole (CzBr$_2$-C2)	-5.88
N-Benzyl-3,6-dibromo-carbazole (CzBr$_2$-Benzyl)	-5.93
Anthracene-9-carbaldehyde (9ACHO)	-5.94
3,6-Diiodo-9H-carbazole (CzI$_2$)	-5.97
3,6-Dibromo-9H-carbazole (CzBr$_2$)	-6.02

Figure S1: Commonly available organic donors considered for this study and their calculated relative strength. (Calculated at B3LYP-GD3/def2tzvp level of theory from the optimised monomeric structure)
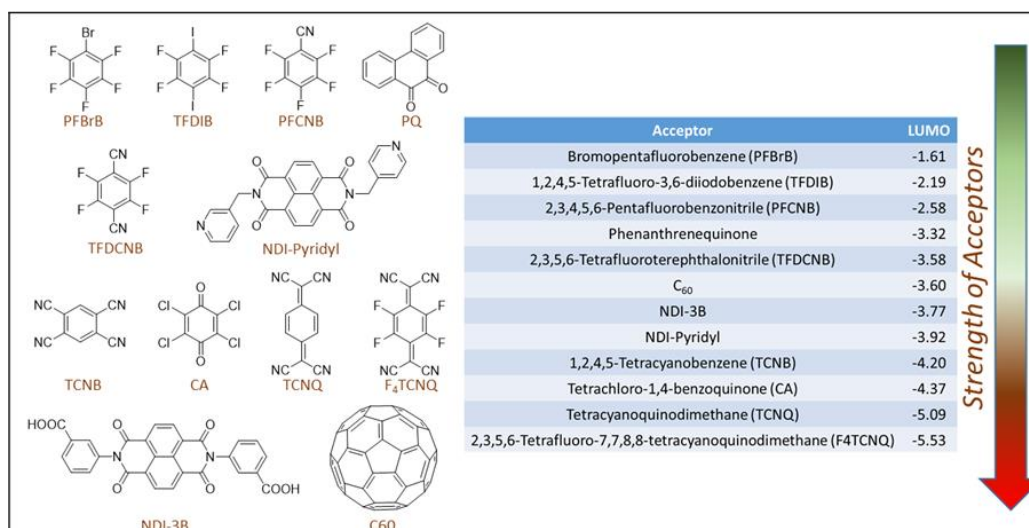
Figure S2: Commonly available organic acceptors considered for this study and their calculated relative strength. (Calculated at B3LYP-GD3/def2tzvp level of theory from the optimised monomeric structure)

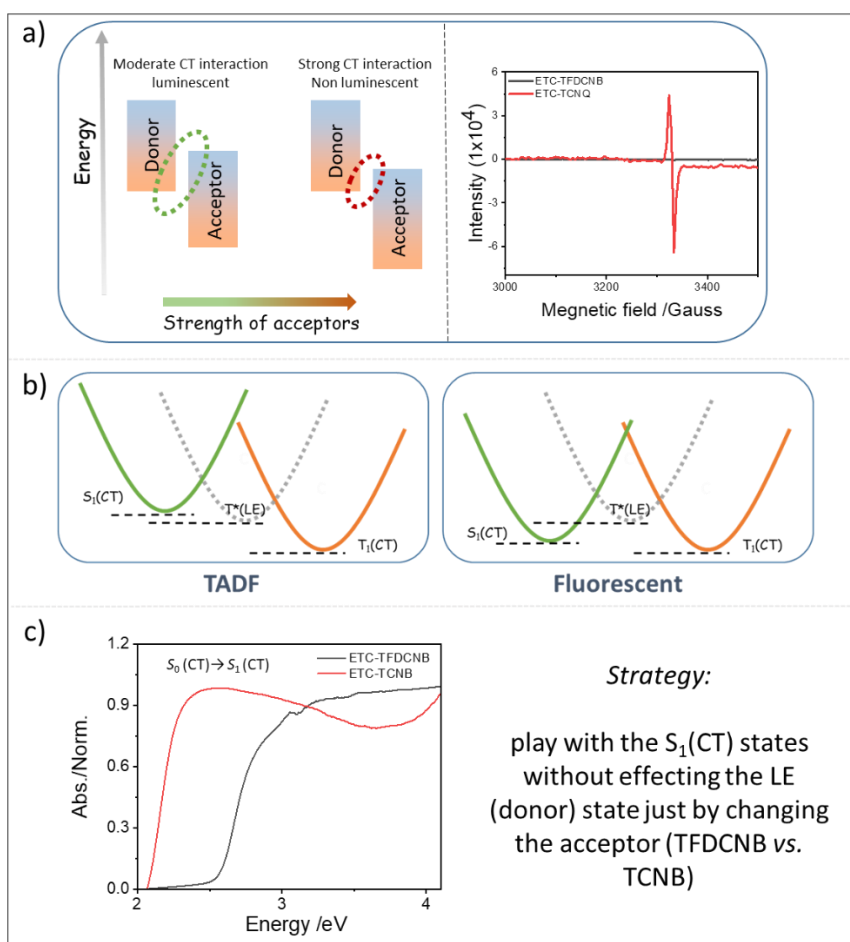**Choice of appropriate donor-acceptor pair for luminescent TADF material:**

Figure S3: Design strategy to choose appropriate donor-acceptor pair for desired functional output a) Strong CT interactions *vs*. moderate CT interaction b) Moderate CT interaction can yield either conventional luminescent or TADF complex c) Electronic absorption spectra of ETC-TFDCNB and ETC-TCNB complex.

Note: In Figure S3 b), it is the size of the energy gap ($\Delta E_{T^*(LE)-S_n(CT)}$) or, in particular, the overlap of T*(LE) and S_n(CT) is more important for efficient RISC (TADF) than the relative position of the states. RISC can be favourable even if the system's LE state(s) lies above the CT state(s), provided there is a tiny energy gap to have sufficient overlap. Fundamentally, it is more the mixing of LE and CT states that makes the RISC process possible. As reported by Monkman and co-workers, RISC is favourable even if the discrete energy level of LE state(s) is above the CT state(s).[4]

Choice of appropriate donor-acceptor pair for desired functional output:
We have carefully screened a list of widely available small molecule D-A conjugates to condense our choice to a few of them to yield TADF. Even though CT complexes show optical and charge carrier transport characteristics different from their conformers, they retain the intrinsic properties of the donor and the acceptor to some extent. For example, cocrystals based on weak fluorescent acceptors like 1,2,4,5-Tetracyanobenzene (TCNB) and 1,2,4,5-Tetrafluoro-3,6-diiodobenzene (TFDIB) are known to yield CT pairs with high PL quantum yield (PLQY). On the other hand, CT complexes formed using strong acceptors like fullerene and F_nTCNQ (n=0,1,2,4) display mainly transport characteristics in line with one component, F_nTCNQ or fullerene. Thus, fine-tuning the degree of charge transfer (DCT) between the D and A units is essential to achieve the best functional output to control the bulk optical properties. Our systematic investigation revealed that moderate charge transfer interactions between D and A units are optimal for obtaining a CT pair with high PLQY. Moreover, emphasis is given to carbazole-derived donor units because of their intrinsic low-lying triplet states and high intersystem crossing rate. Out of our list (Figure S1), carbazole(s) are the best-suited donor entities for yielding luminescent TADF charge transfer complexes with appropriate acceptors.

Synthesis Procedure for Carbazole (Cz):
Carbazole (Cz) was synthesised following the procedure described in Scheme S1.[5]
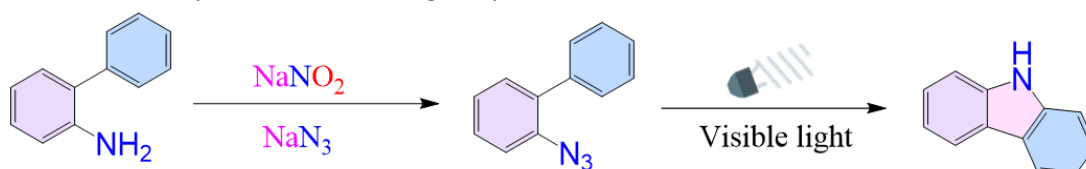
Scheme S1: Synthetic procedure of carbazole (Cz)

2-Azidobiphenyl was synthesised from 2-aminophenyl using traditional diazotisation, followed by nucleophilic aromatic substitution by sodium azide. In a round-bottom flask, 2-Aminobiphenyl (0.250 g, 1.48 mmol, 1.0 equivalent) was dissolved in 10 mL of HOAc and 5 mL of H_2O and chilled in an ice bath. $NaNO_2$ (0.142 g, 2.07 mmol, 1.4 equivalent) was added slowly, and the resulting mixture was stirred at 0 °C for one hour. NaN_3 (0.144 g, 2.22 mmol, 1.5 equivalent) was added slowly, and the resulting mixture was warmed to ambient temperature and stirred for 60 minutes. The solution was diluted with 20 mL of water and 20 mL of CH_2Cl_2 and basified by the slow addition of K_2CO_3 until bubbling ceased. The phases were separated, and the aqueous phase was extracted with an additional 2×20 mL of CH_2Cl_2. The combined organic phases were washed with 1×20 mL of water and 1×20 mL of brine. The resulting organic phase was collected and dried over Na_2SO_4 and filtered. The filtrate was concentrated in a vacuum to get the desired azide. The above procedure was repeated several times to produce sufficient 2-Azidobiphenyl. Yield~98%

After that, 0.585 g (3.0 mmol) of 2-Azido biphenyl, 0.3 g silica gel, 20 mL water and 20 mL of acetone were added to a 150 mL reaction tube. The mixture was stirred for 72 hours with light irradiation. The biphasic solution was diluted with 25 mL of water and 25 mL of CH_2Cl_2 and separated. The aqueous phase was extracted with 3×10 mL of CH_2Cl_2. The organic phase was dried over Na_2SO_4 and filtered. The filtrate was concentrated in a vacuum to afford the crude product. The crude product was purified by column chromatography on silica gel (petroleum ether and ethyl acetate gradient) to give the desired product. The procedure was repeated several times to produce a sufficient amount of carbazole. Yield~40%

Synthesis Procedure for Ethylcarbazole (ETC):

Ethylcarbazole (ETC) was synthesised following the procedure described in Scheme S2.
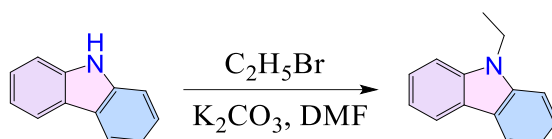
Scheme S2: Synthetic procedure of Ethylcarbazole (ETC)

In a 250 mL round bottom flask, 250 mg of carbazole (Cz) (1 equivalent) is dissolved in 10 mL dry dimethylformamide (DMF). Next, microwave-activated potassium carbonate (15 equivalent) is added to the reaction mixture under the argon atmosphere. The solution turns yellowish. After 30 minutes, ethyl bromide (1.5 equivalent) is added to the reaction mixture and stirred at 120 ^{0}c for 24 hours under an argon atmosphere. After the reaction, deionised water is added to the reaction mixture to get a white residue. The residue is washed 2-3 times with diethyl ether/water to remove the DMF. The product is recrystallised from ethyl acetate/methanol solution. The yield of the reaction is ~95%.

Characterisation of Carbazole (Cz):
^{1}H NMR (500 MHz, DMSO) δ [ppm]: δ 11.22 (s, 1H), 8.10 (d, J = 7.7 Hz, 2H), 7.53 – 7.41 (m, 2H), 7.37 (t, J = 7.9 Hz, 2H), 7.14 (t, J = 7.3 Hz, 2H). Solvent residual peak of DMSO: δ=2.50; Water in DMSO: δ=3.33 (s); CH_2Cl in DMSO δ=5.76 (s).[5]
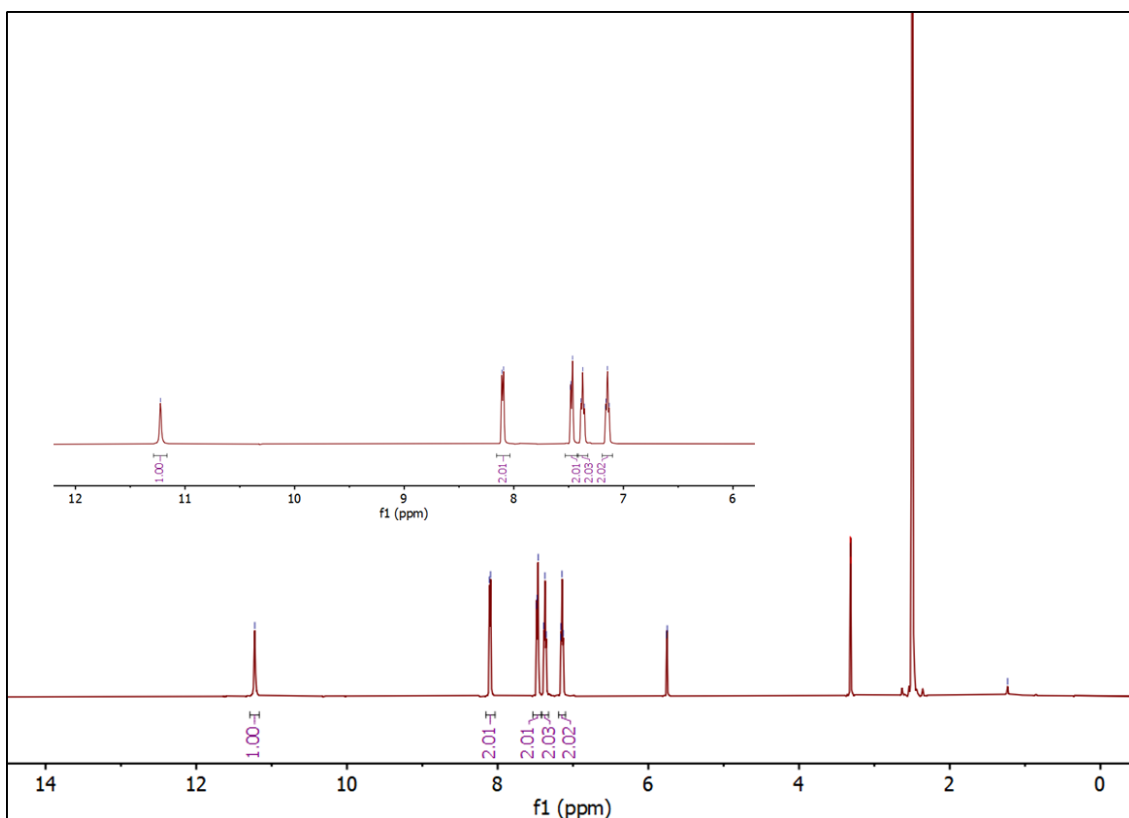
Figure S4: ^{1}H NMR spectrum of Carbazole (Cz).

^{13}C NMR (126 MHz, DMSO) δ [ppm]: δ 135.54 (2C), 125.45 (2C), 122.34 (2C), 120.10 (2C), 118.43 (2C), 110.88 (2C) ppm. Solvent residual peak of DMSO: δ=39.52; CH$_2$Cl in DMSO δ=54.84 (s).[6]
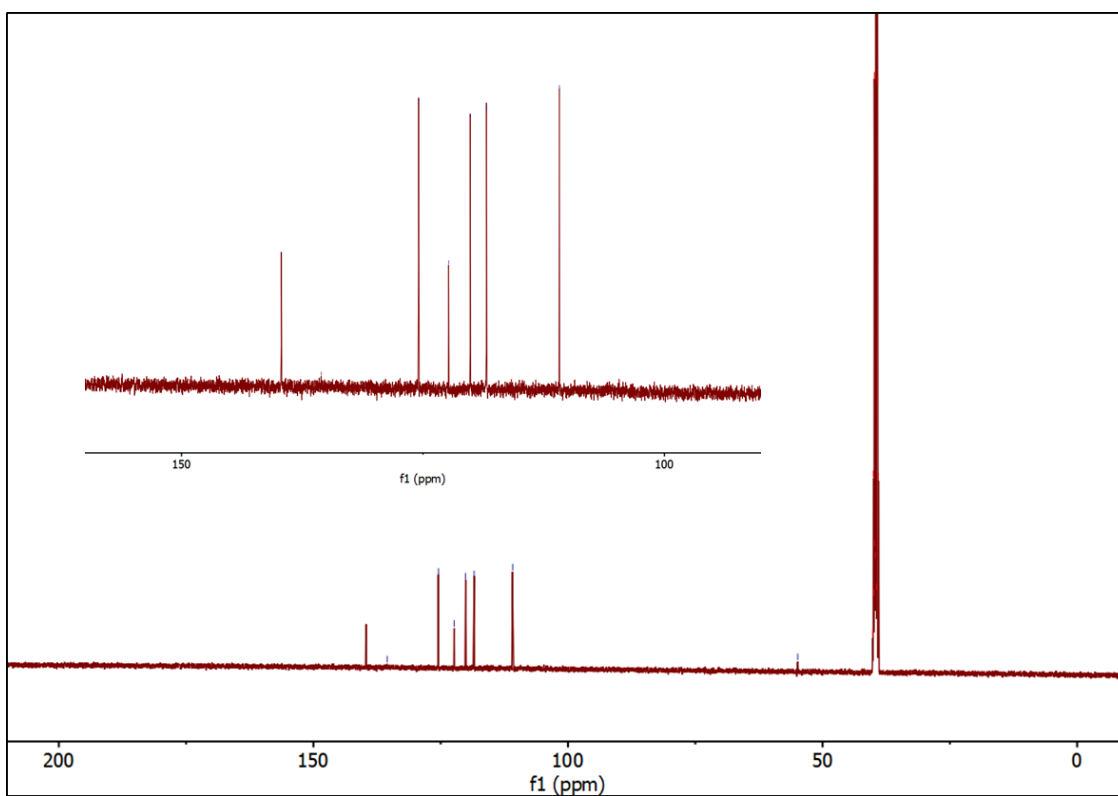

Figure S5: ^{13}C NMR spectrum of Carbazole (Cz).

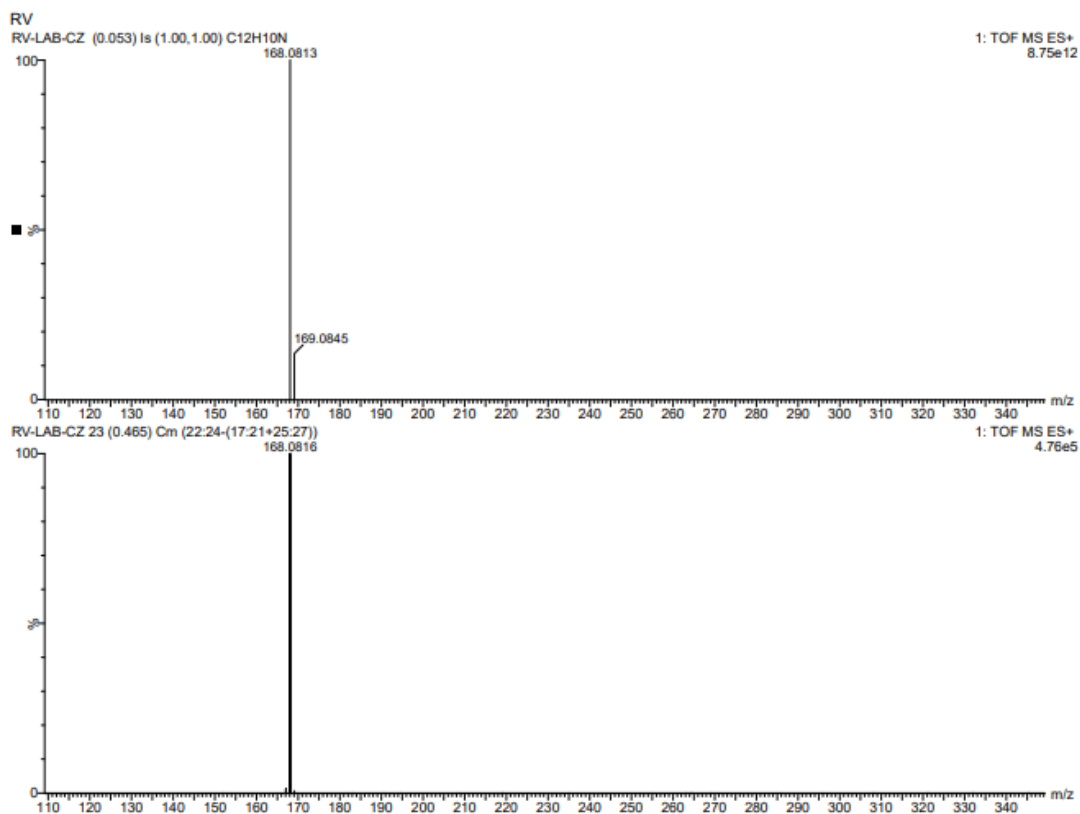**HRMS analysis of Cz:** m/z calculated=168.0813 (100%) Found= 168.0816 (100%)

Figure S6: HRMS of Carbazole (Cz). (Top: simulated; bottom: experimentally found)

HPLC Analysis of Cz: HPLC analysis was recorded using acetonitrile (MeCN), and water in an 80:20 ratio was used as the solvent mixture system and monitored from 210 nm to 460 nm.
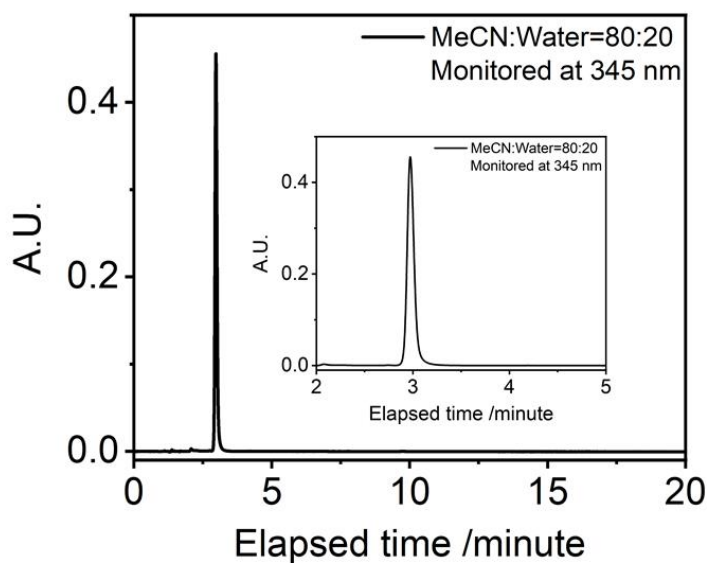
Figure S7: HPLC profile of Carbazole (Cz) in acetonitrile: H_2O (80:20) mixture, monitoring at 345 nm.

Elemental Analysis of Cz: *Calculated*: C: 86.2, H: 5.4, N: 8.4 *Found*: C: 86.4, H: 5.0, N: 8.6

Characterisation of Ethylcarbazole (ETC):

¹H NMR (500 MHz, DMSO) δ [ppm]: δ 8.16 (dt, *J* = 7.8, 1.0 Hz, 2H), 7.61 (d, *J* = 8.2 Hz, 2H), 7.46 (ddd, *J* = 8.3, 7.0, 1.2 Hz, 2H), 7.24 – 7.17 (m, 2H), 4.45 (q, *J* = 7.1 Hz, 2H), 1.32 (t, *J* = 7.1 Hz, 3H).
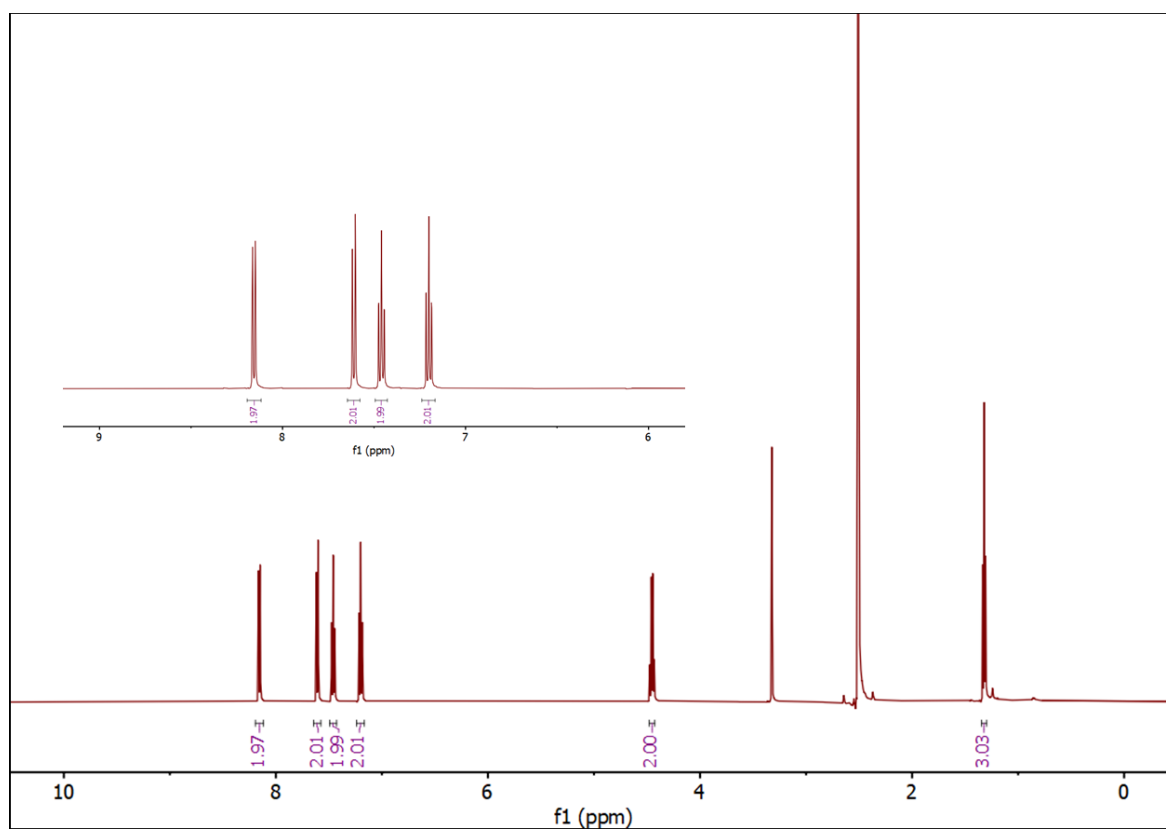

Figure S8: ¹H NMR spectrum of Ethylcarbazole (ETC)

¹³C NMR (126 MHz, DMSO) δ [ppm]: δ 139.46 (2C), 125.63 (2C), 122.10 (2C), 120.28 (2C), 118.61 (2C), 109.01 (2C), 36.86 (2C), 13.63 (3C).
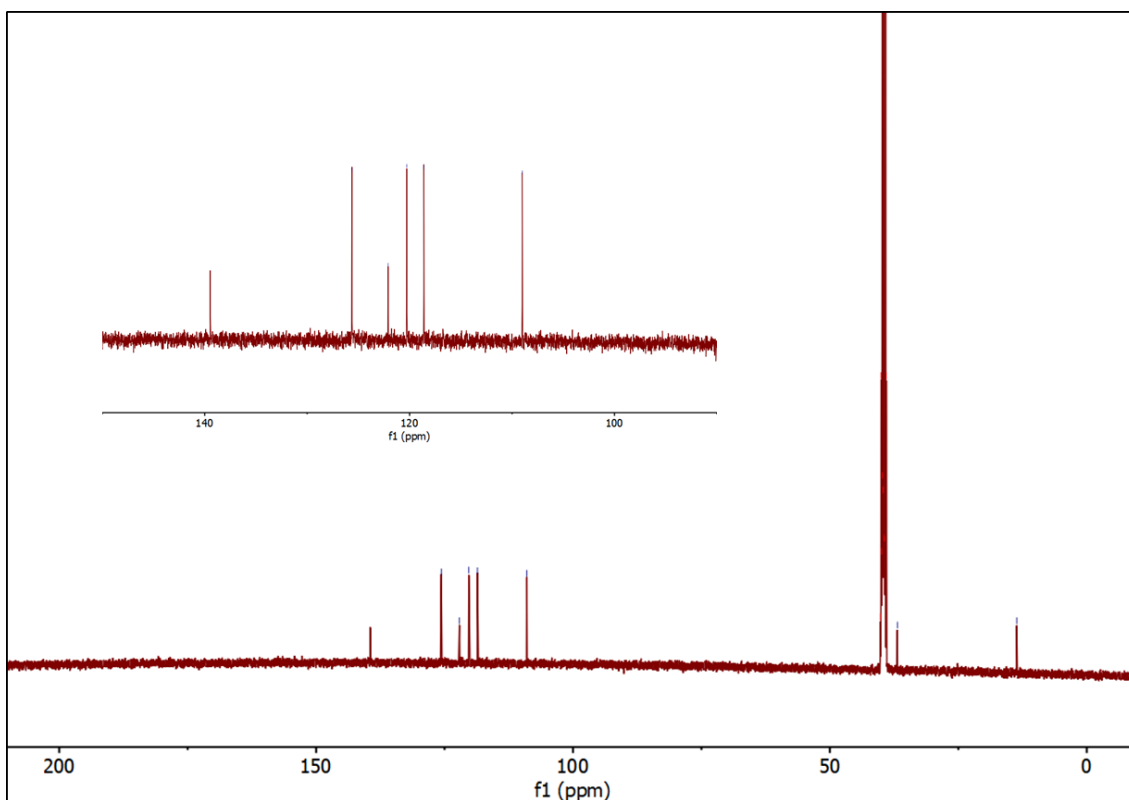
Figure S9: ^{13}C NMR spectrum of Ethylcarbazole (ETC)

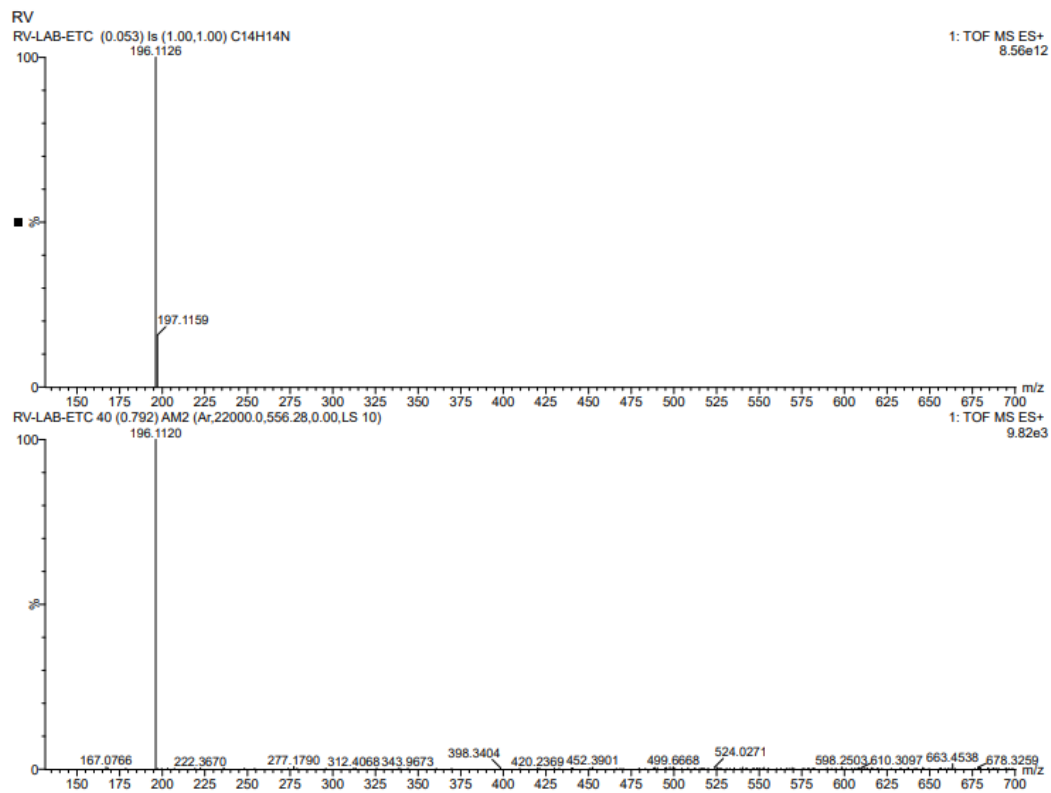**HRMS analysis of ETC:** m/z calculated= 196.1126 (100%) Found=196.1120 (100%)

Figure S10: HRMS of Ethylcarbazole (ETC).

HPLC Analysis of ETC: HPLC analysis was recorded using acetonitrile (MeCN), and water in an 80:20 ratio was used as the solvent mixture system and monitored from 210 nm to 460 nm.
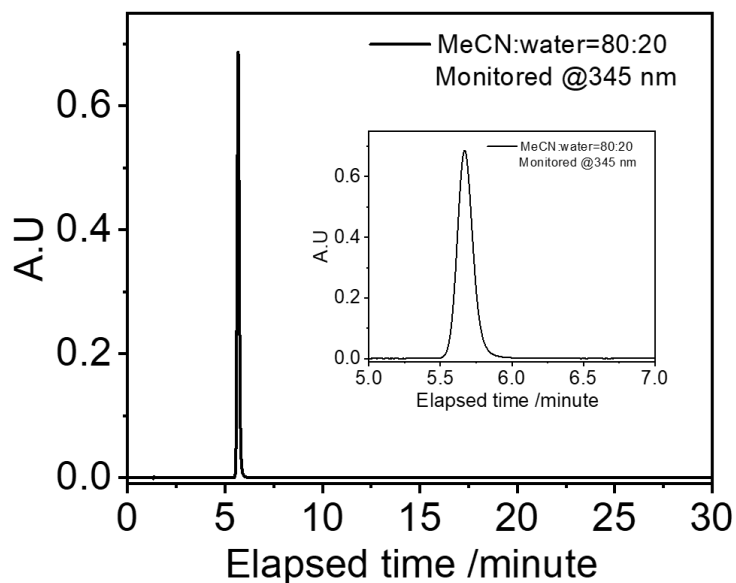

Figure S11: HPLC profile of ETC in acetonitrile: H_2O (80:20) mixture, monitoring at 345 nm.

Melting point measurement: Reported=65-70 °C. Found = ~69 °C (from DSC analysis)

Elemental Analysis of ETC: *Calculated*: C: 86.1, H: 6.7, N: 7.2 *Found*: C: 86.1, H: 6.5, N: 7.2

Preparation of charge transfer (CT) complex: The CT complexes are prepared using the liquid-assisted grinding (LAG) technique. A few drops of acetonitrile solvent are used to grind the donor (D) and acceptor (A) mixture. (Figure S12) In a typical experiment, the donor and the acceptor molecules are mixed in a 1:1 molar ratio, and the CT complex is prepared through liquid-assisted grinding. Initial screenings to confirm the formation of the CT complex are done by monitoring the change of colour in the resulting mixture from that of the corresponding conformers. In the case of the ETC-TFDCNB complex, both ETC and TFDCNB are colourless solids, while the complex formed is greenish-yellow. Single crystal of ETC-TFDCNB is grown by slow solvent evaporation from a supersaturated ethanol solution of grounded powder. Single crystals suitable for X-ray crystallography and photophysical studies are obtained from the above solution in 2 to 3 days. As shown in Figure S13, PXRD data indicates the formation of a complex as the PXRD pattern of the as-prepared grounded complex is different from that of the two conformers.
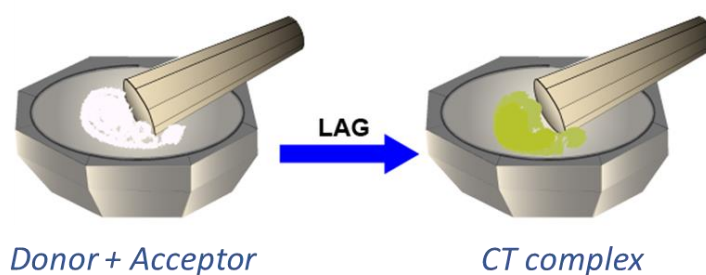

Donor + Acceptor   *CT complex*

Figure S12: Schematic representation of the liquid-assisted grinding (LAG) method used to synthesise the charge transfer complex.
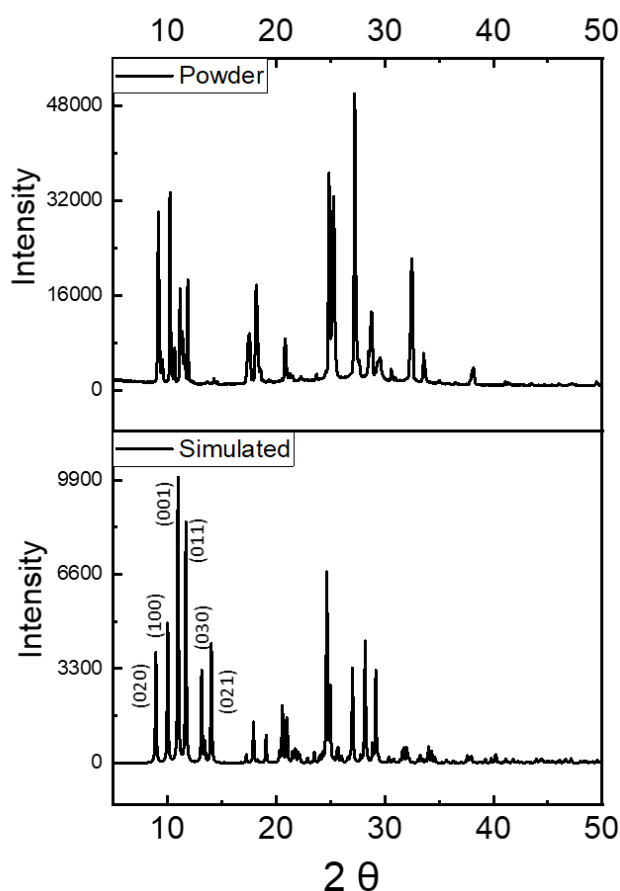
Powder X-ray diffraction (PXRD):

Figure S13: Comparison of PXRD pattern: bottom) simulated from the crystal structure of ETC-TFDCNB; top) as prepared grounded ETC-TFDCNB powder.

Thermal analysis of ETC-TFDCNB complex:

The TGA thermogram (Figure S14) shows that the ETC-TFDCNB co-crystal possess a different thermal behaviour and decomposition temperature in comparison to its individual components ETC and TFDCNB. ETC has a higher decomposition temperature (~ 200 °C) than TFDCNB (~ 150 °C). As anticipated, the cocrystal ETC-TFDCNB has a decomposition temperature (~ 180 °C) in between that of ETC and TFDCNB. The TGA graphs are recorded at a 5 °C/minute heating rate.

The DSC thermogram of the individual components, ETC and TFDCNNB, showed a melting endotherm maximum at 69 °C and 197 °C respectively, whereas the ETC-TFDCNB complex exhibits a melting endotherm maximum at 83 °C, which is in between that of the ETC and TFDCNB indicate the formation of the cocrystal. Moreover, we observed two endothermic transitions with extremely low (ΔH = 2.7 J/g and ΔH = 4.4 J/g) just before the melting point of the ETC-TFDCNB complex.) This is attributed to crystal-to-crystal phase transition (induced by thermally activated dislocation of molecules) in the CT complex. The DSC graphs are recorded at a 5 °C/minute heating and cooling rate. (Figure S15)
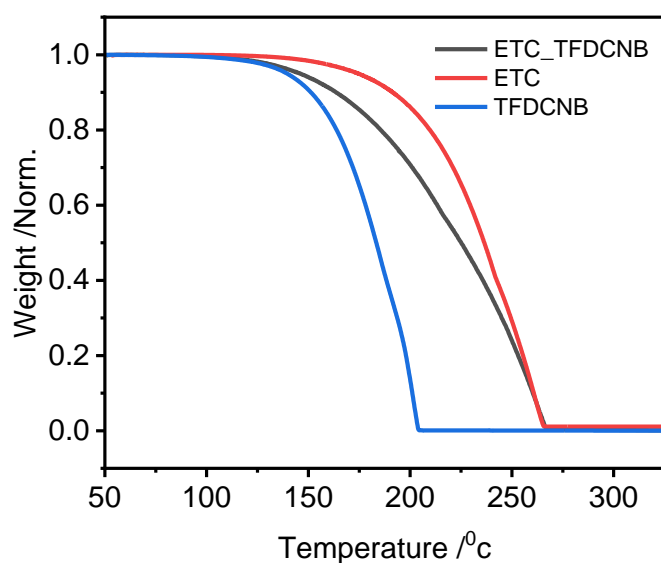
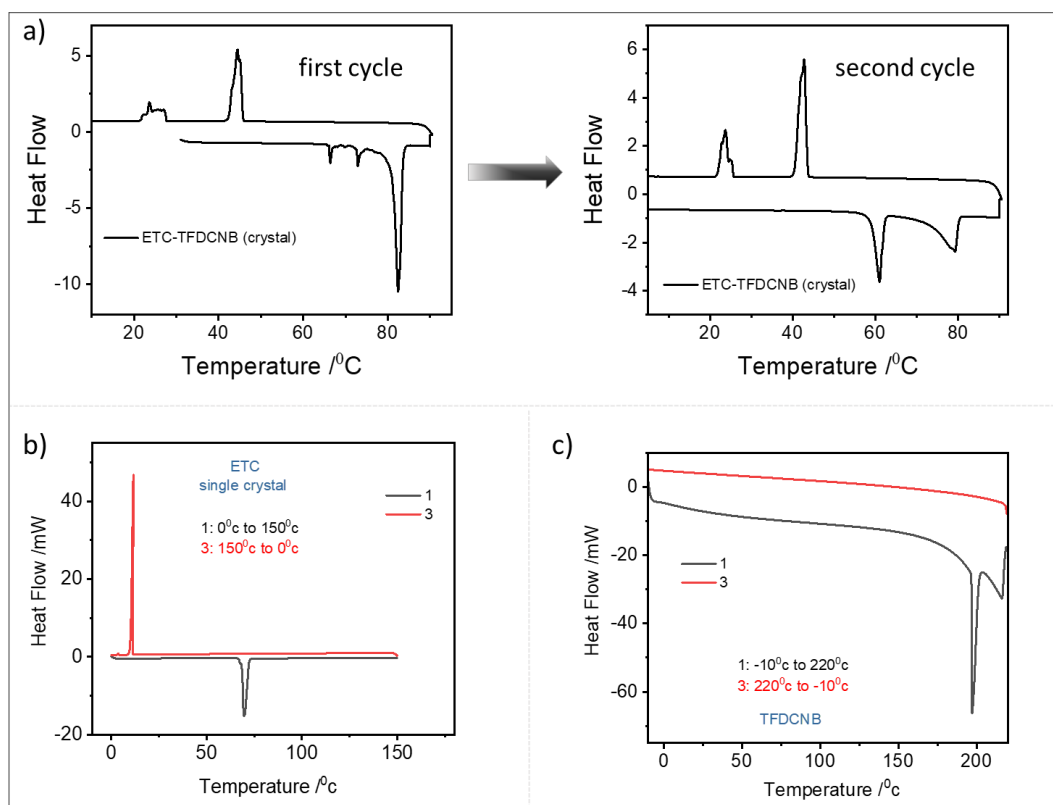**Figure S14:** Thermogravimetric analysis (TGA) plot of ETC, TFDCNB and ETC-TFDCNB CT complex.

Figure S15: Differential Scanning Calorimetry (DSC) thermogram of a) ETC-TFDCNB CT complex b) ETC and c) TFDCNB.

Crystallinity of drop-casted films:

The drop casted films were prepared on cleaned quartz or Silicon substrates. The drop-casted films are highly crystalline and retain the distinctive CT character of the co-crystal evident from microscopic data, as shown below. Needle-like crystalline domains with a characteristic birefringence are evident in Figure S16 a. The topology was confirmed from the SEM analysis (Figure S16b), and aligned crystalline domains were evident. Also, the colour of such film was similar to that of the single crystals and characteristic bright CT emission is also observed from the drop-casted film.
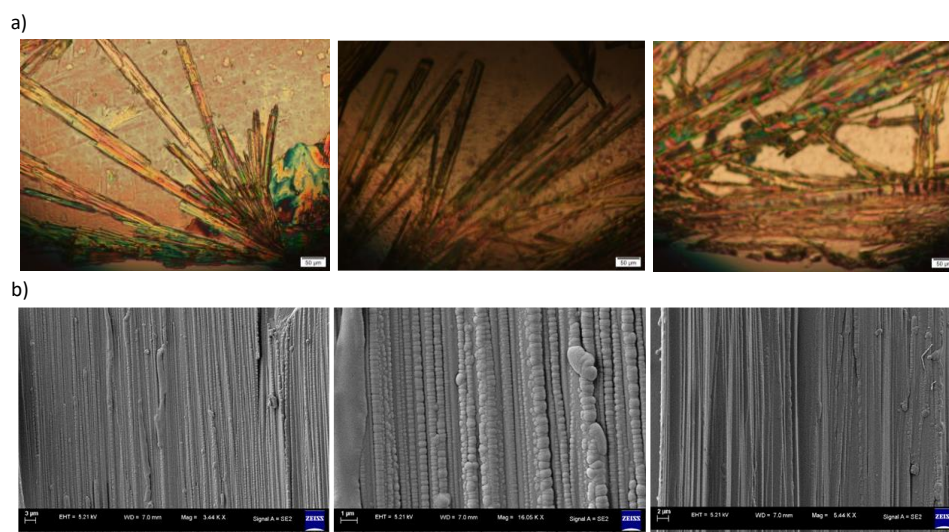

Figure S16: Optical microscopy image of drop-casted films of ETC-TFDCNB complex; b) Scanning electron microscopy (SEM) images of drop-casted films of ETC-TFDCNB complex.

Single crystal XRD cell parameter ETC-TFDCNB:

Room Temperature (300 K)	Low Temperature (100 K)
Formula: $C_{18} H_{13} F_2 N_2$ Space Group: P 2_1/c (monoclinic) a=9.2 A^0, b=19.4 A^0, c=8.4 A^0 α=90.0^0 β=108.9^0 γ=90.0^0	Formula:$C_{18} H_{13} F_2 N_2$ Space Group: P 2_1/c (monoclinic) a=9.2 A^0, b=19.7 A^0, c=8.6 A^0 α=90.0^0 β=107.4^0 γ=90.0^0

Table S1: Crystallographic cell parameters for ETC-TFDCNB, obtained from SCXRD at room and low temperatures.
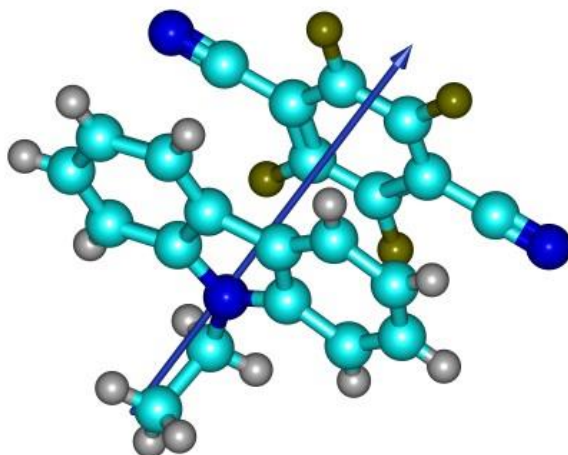
Static dipole moment:

Figure S17: Static dipole moment (SDM) vector for the ETC-TFDCNB complex.

Electronic transitions:

TD-DFT calculations were performed using Gaussian 16 software.[8] TD-DFT calculation was done at TPSSh-GD3BJ/def2tzvp level of theory and employing ultrafine numerical integration grid (pruned 99,590). Obtained results from TD-DFT were analysed using GaussSum software.
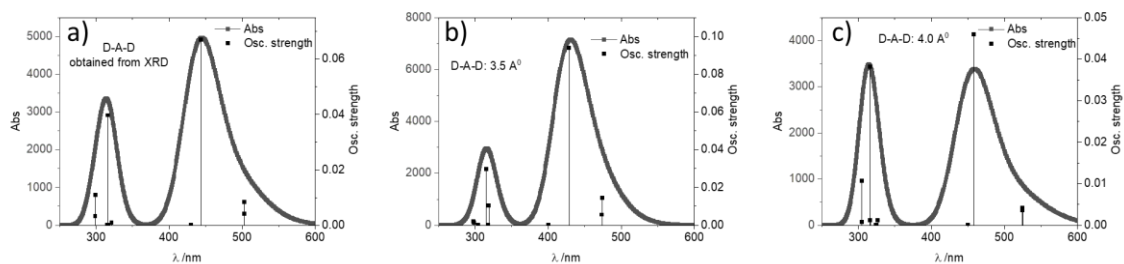

Figure S18: simulated electronic absorption spectra of Donor (D)-Acceptor (A)-Donor (D) unit at different distances between donor and acceptor unit using TD-DFT (TPPSh-D3BJ/Def2TzVP) method

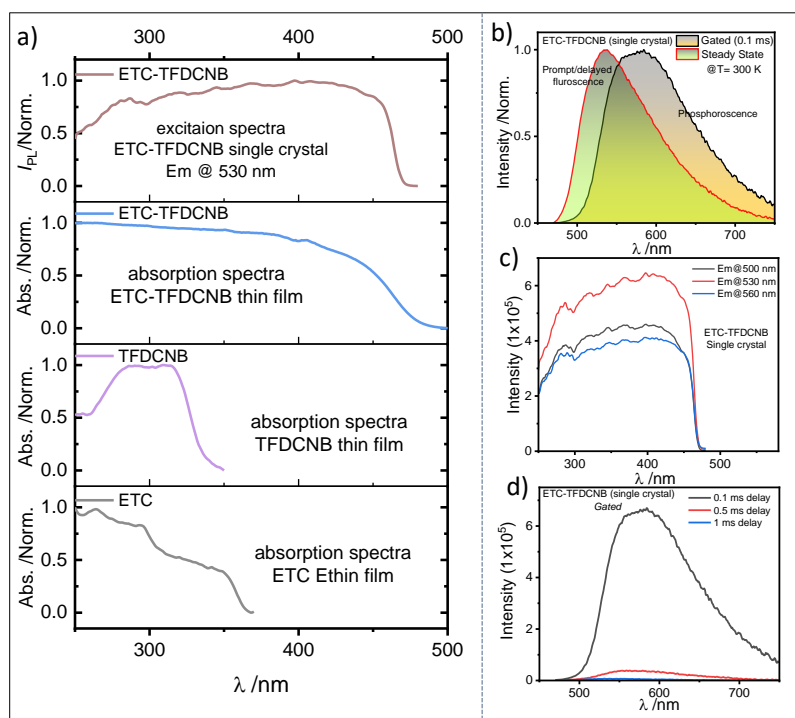**Absorption, emission and excitation spectrum of ETC-TFDCNB:**

Figure S19: a) From top to bottom: excitation spectra of ETC-TFDNB single crystal (emission at 530 nm); UV-Vis absorption spectra of ETC-TFDCNB thin film; UV-Vis absorption spectra of TFDCNB thin film; UV-Vis absorption spectra of ETC thin film. All spectra are normalised at maxima. b) Steady-state and gated PL emission spectra for a single crystal at 300 K upon excitation at 440 nm. c) ETC-TFDCNB single crystal excitation spectra (emission collected at 500 nm, 530 nm and 560 nm). d) Gated PL emission spectra for a single crystal at 300 K upon excitation at 440 nm at different delay times.

Polymer-doped ETC-TFDCNB film:

1. Polystyrene (PS): 50 mg of polystyrene was dissolved in 1 ml of toluene to make a homogeneous solution (heated@80^{0}c). Then, 5 mg of the CT complex was dissolved in 1 ml of toluene. Both solutions were mixed to get a uniform solution.
2. Poly (methyl methacrylate) (PMMA): 50 mg of PMMA was dissolved in 1 ml of $CHCl_3$ to make a homogeneous solution. Then, 5 mg of the compound was dissolved in 1 ml $CHCl_3$. Both solutions were mixed to get a uniform solution.

The above solution was cast on a quartz substrate, and the absorbance and PL spectrum were recorded.
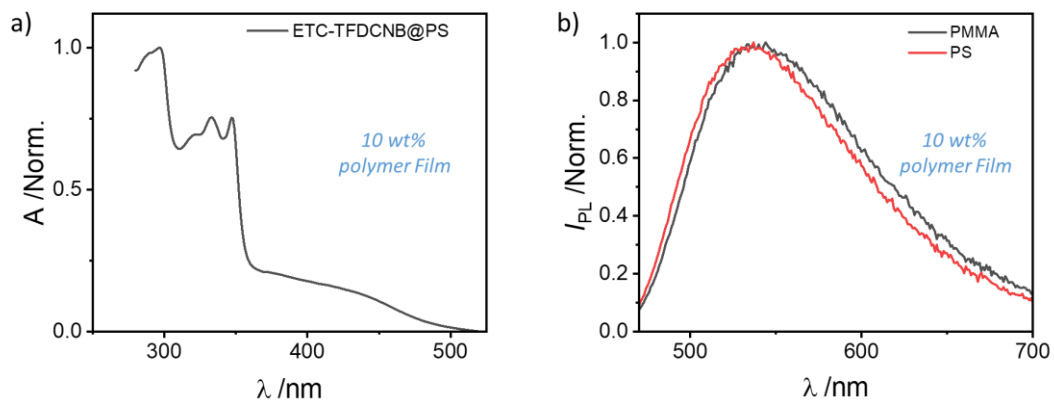
Figure S20: a) UV-Vis absorption spectra of 10 wt% ETC-TFDCNB polystyrene film at ambient conditions. b) Normalized Steady-state PL spectra 10 wt% ETC-TFDCNB polystyrene and PMMA film at ambient conditions.

Steady-state emission and excitation spectra of ETC-TFDCNB thin film at variable temperatures:
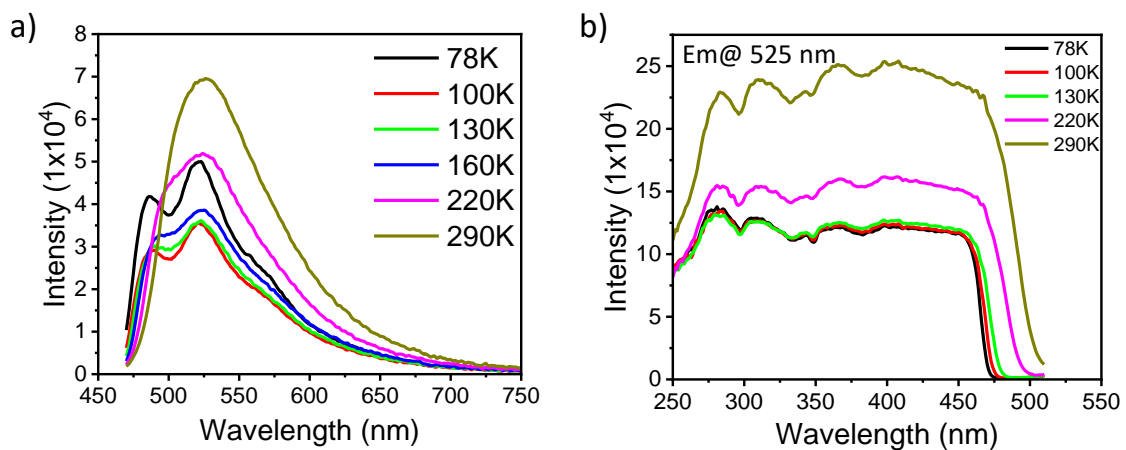

Figure S21: ETC-TFDCNB film - state a) emission spectra at different temperature (excited @440 nm), b) temperature dependent excitation spectra at emission @525 nm.

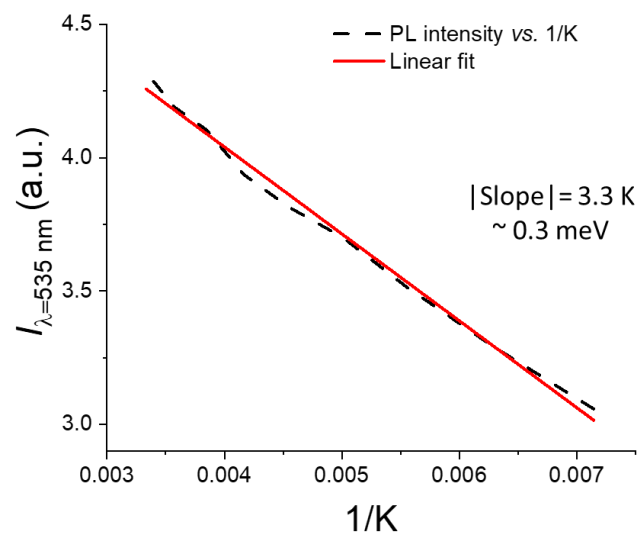**Activation energy barrier calculation:**

Figure S22: Activation energy calculation of ETC-TFDCNB from the slope analysis

Photoluminescence spectra of DTBC-TFDCNB CT complex and DTBC alone:

DTBC-TFDCNB complex shows thermally activated delayed fluorescence (TADF) similar to ETC-TFDCNB.
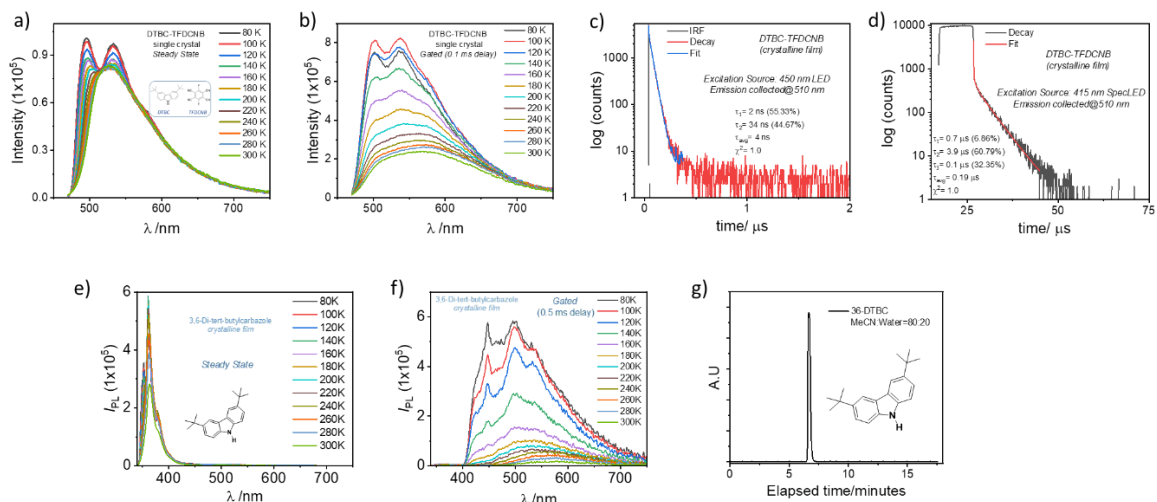

Figure S23: a) Steady-state emission spectra for DTBC-TFDCNB crystal at variable temperature; b) gated (0.1 ms initial delay) emission spectra for DTBC-TFDCNB crystal at variable temperature; c) prompt lifetime decay profile of ETC-TFDCNB film at room temperature; d) delayed lifetime decay profile of DTBC-TFDCNB film at room temperature; PL emission spectrum of ETC crystalline film e) steady state and f) time-resolved (initial delay=0.5 ms); g) HPLC profile of Carbazole (DTBC) in acetonitrile: H_2O (80:20) mixture, monitoring at 345 nm.

Photoluminescence spectra of Pyrene-TFDCNB CT complex:

Pyrene-TFDCNB complex also shows thermally activated delayed fluorescence (TADF) behaviour. The locally excited Pyrene triplet state is the bridging state between S_1(CT) and T_1(CT) of the Pyrene-TFDCNB complex.
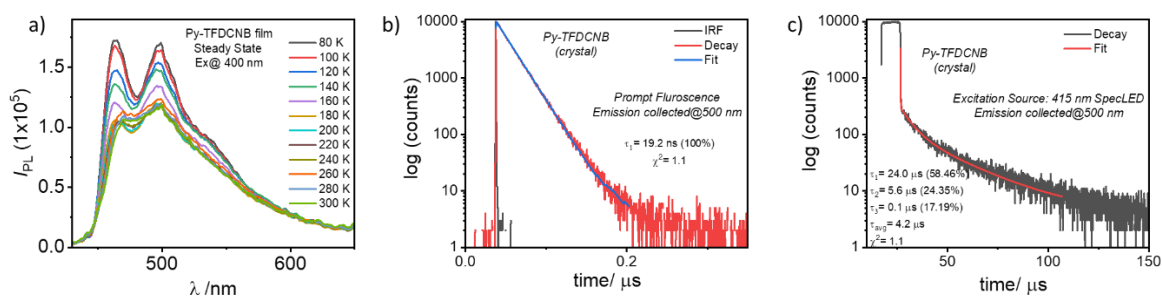

Figure S24: a) Steady-state emission spectra for Pyrene-TFDCNB crystal at variable temperature; b) prompt lifetime decay profile of Pyrene-TFDCNB crystal at room temperature; c) Delayed lifetime decay profile of Pyrene-TFDCNB film at room temperature.

Photoluminescence spectra of ETC-TCNB CT complex:

ETC-TCNB CT complex forms a fluorescent complex as the locally excited triplet state could not facilitate the (R)ISC process as it lies energetically way above the charge transfer states.
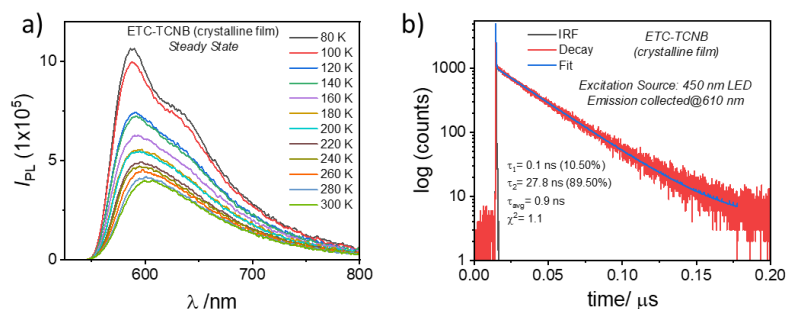

Figure S25: a) Steady-state emission spectra for ETC-TCNB crystal at variable temperature. c) Prompt lifetime decay profile of ETC-TCNB film at room temperature.

Photoluminescence spectra of other CzBr$_2$-C6-TFDCNB CT complex:

CzBr$_2$-C6-TFDCNB CT complex forms a luminescent exciplex. The extent of charge transfer is significantly less in this pair as CzBr$_2$-C6 is a weak donor compared to ETC and DTBC. Thus, no ground state charge transfer complex is formed.
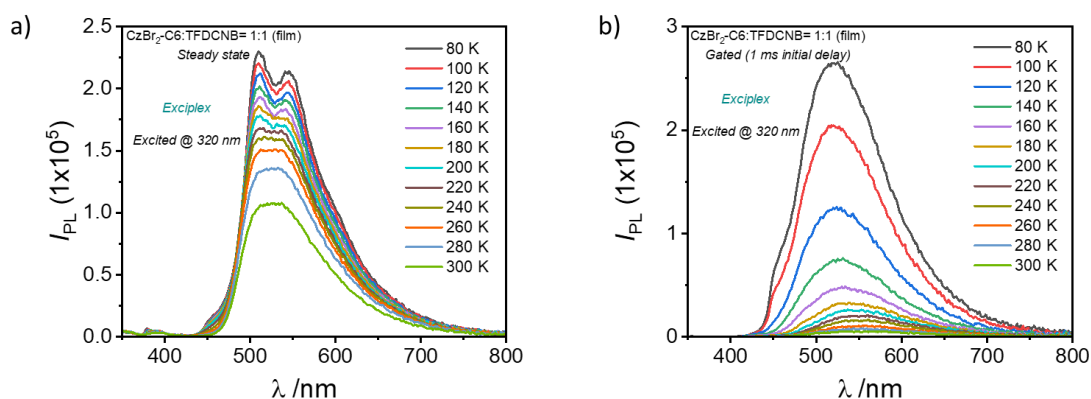
Figure S26: a) Steady-state emission spectra for CzBr$_2$-C6-TFDCNB complex at variable temperature; b) gated (0.1 ms initial delay) emission spectra for CzBr$_2$-C6-TFDCNB complex at variable temperature.

BFDH crystal morphology and face indexing of ETC-TFDCNB: BFDH crystal morphology of ETC-TFDCNB was generated using Mercury 2020.2.0.

Figure S27: Face indexing image and BFDH morphology of ETC-TFDCNB crystal.

Mechanical deformation of ETC-TFDCNB crystal:

Figure S28: Mechanical deformation of a) thin and b) thick crystals of ETC-TFDCNB after exfoliation.

Histogram plots of ETC-TFDCNB evaluated from performed nanoindentation measurements:
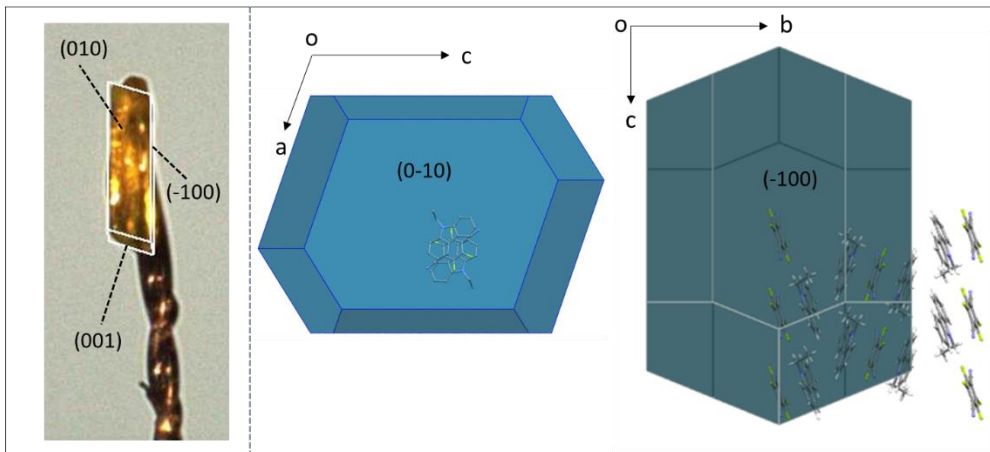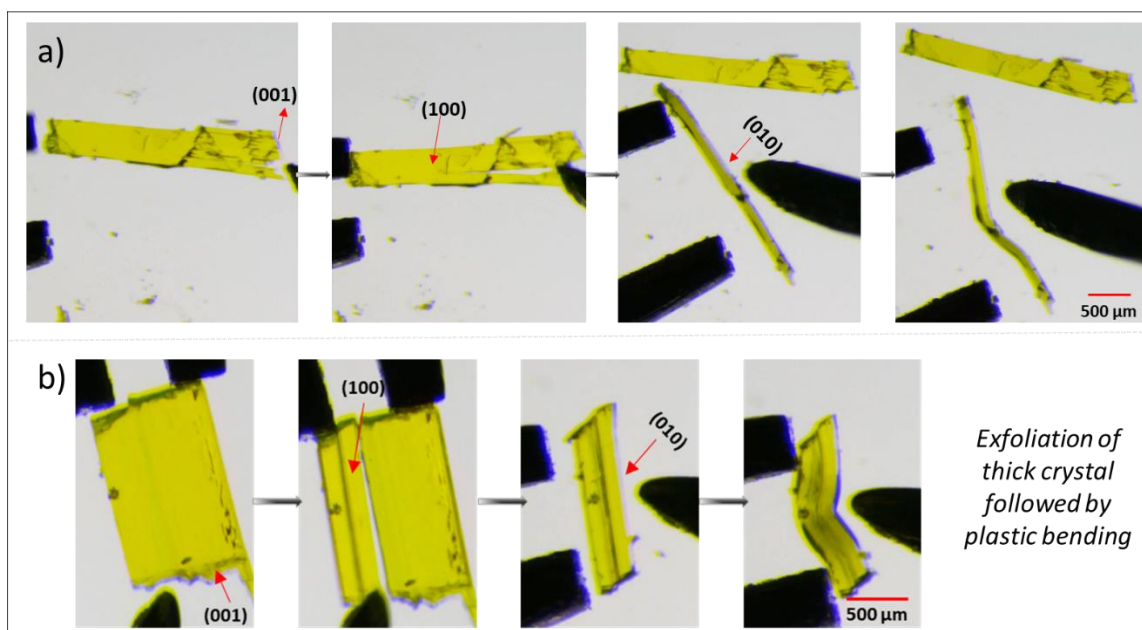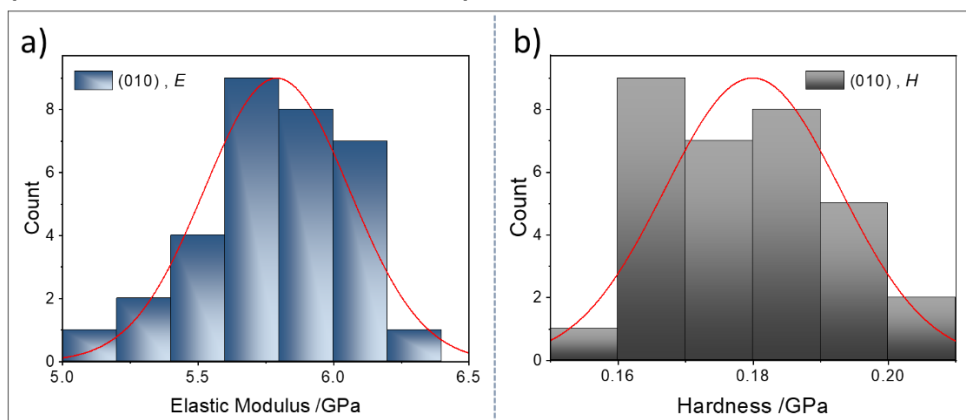

Figure S29: Histogram of elastic modulus (a) and hardness (b) obtained from several indentations performed on different samples of ETC-TFDCNB on the (010) face at 5 mN load.
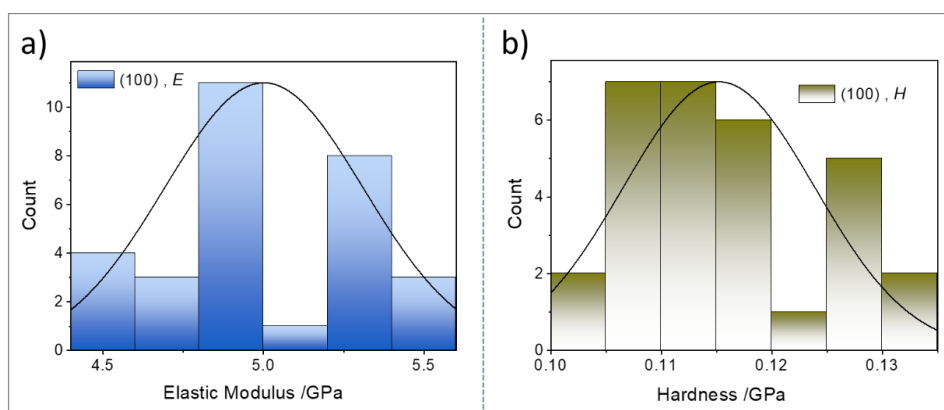
Figure S30: Histogram of elastic modulus (a) and hardness (b) obtained from several indentations performed on different samples of ETC-TFDCNB on the (100) face at 5 mN load.

Energy frameworks analysis of ETC-TFDCNB: Interaction energies were calculated at B3LYP/6-31G(d,p) level of theory using CrystalExplorer17.5 software.[6]

Dimeric pair	Coulomb Energy	Dispersion Energy	Total Energy	Energy Values (kJ/mol)
D-A (d=3.57 Å)	E_{ele}= -21.0 kJ/mol	E_{dis}= -68.1 kJ/mol	E_{tot}= -54.6 kJ/mol	E_{ele}= -21.0 E_{pol}= -7.5 E_{dis}= -68.1 E_{rep}= -52.7 E_{tot}= -54.6
D-D (d=5.70 Å)	E_{ele}= -21.0 kJ/mol	E_{dis}= -68.1 kJ/mol	E_{tot}= -54.6 kJ/mol	E_{ele}= -9.5 E_{pol}= -1.9 E_{dis}= -40.2 E_{rep}= 29.8 E_{tot}= -28.1

Figure S31: Interaction energy and energy framework of ETC-TFDCNB crystal along different directions with a 100 energy scale factor and a zero energy threshold.

Crystal packing of DTBC-TFDCNB:

DTBC-TFDCNB are brittle due to the absence of slip planes or any restorable interactions.
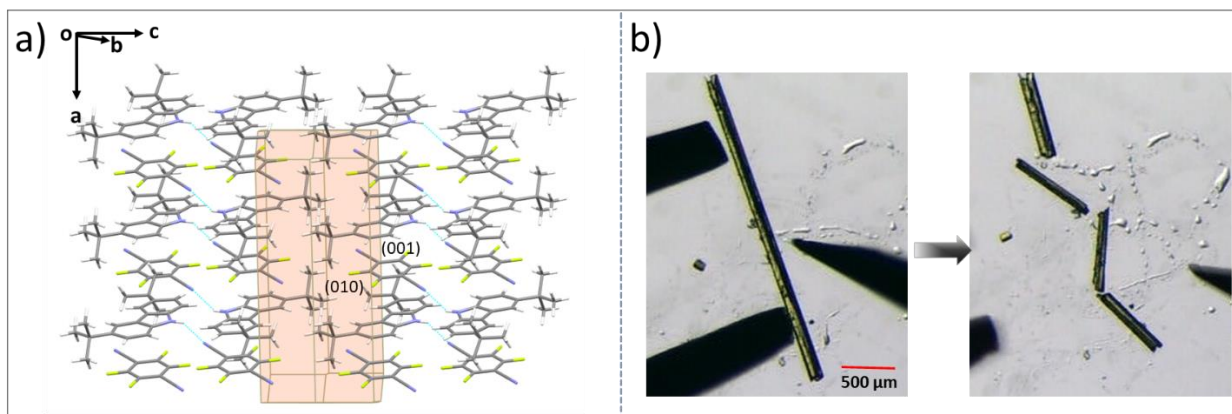
Figure S32: (a) Crystal packing of DTBC-TFDCNB with BFDH morphology shows that it contains moderate N-H⋯N hydrogen bonding interactions (d/Å, ϑ/°: 2.32Å, 147.47°) and no weak interacting plane or restorative interactions present in the structure for plastic or elastic deformation. (b) The DTBC-TFDCNB crystals fracture in a brittle manner upon applying mechanical stress.

Crystallographic information:

ETC-TFDCNB (100 K)

Temperature (K)	100.00(13)
Crystal System	Monoclinic
Space group	$P2_1/c$
a/ Å	9.21813(19)
b/Å	19.4553(3)
c/Å	8.39007(17)
α/°	90
β/°	108.890(2)
γ/°	90
V/ Å^3	1423.65(5)
D_c/ g cm^{-3}	1.378
μ /mm^{-1}	0.834
$F(000)$	612
θ range/°	4.545-68.226
Reflections collected	9254
Unique reflections	2566
reflections I > 2σ(I)	2164
R_{int}	0.0334
Goodness of fit (F^2)	1.052
$R1$ ($I > 2\sigma(I)$)	0.0375
$wR2(I > 2\sigma(I))$	0.0984
CCDC No.	2260509

ETC-TFDCNB (293 K)

Temperature (K)	293(2)
Crystal System	monoclinic
Space group	$P2_1/c$
a/ Å	9.2342(3)
b/Å	19.7739(4)
c/Å	8.5738(3)
α/°	90
β/°	107.396(3)
γ/°	90
V/ Å^3	1493.94(8)
D_c/ g cm^{-3}	1.313
μ /mm^{-1}	0.795
$F(000)$	612
θ range/°	4.472-68.251
Reflections collected	36060
Unique reflections	2718
reflections I > 2σ(I)	2359
R_{int}	0.0389
Goodness of fit (F^2)	1.076
$R1$ ($I > 2\sigma(I)$)	0.0379
$wR2(I > 2\sigma(I))$	0.1091
CCDC No.	2260510

ETC-TCNQ

Temperature (K)	100.00(10)
Crystal System	triclinic
Space group	P-1
a/ Å	6.6187(2)
b/Å	9.1334(3)
c/Å	16.8821(5)
α/°	95.636(3)
β/°	94.087(2)
γ/°	94.166(3)
V/ Å^3	1009.76(5)
D_c/ g cm^{-3}	1.314
μ /mm^{-1}	0.636
$F(000)$	416
θ range/°	2.638-68.548
Reflections collected	14382
Unique reflections	3652
reflections I > 2σ(I)	3098
R_{int}	0.0731
Goodness of fit (F^2)	1.051
$R1$ ($I > 2\sigma(I)$)	0.0786
$wR2(I > 2\sigma(I))$	0.2065

CCDC No.	2260511

DTBC-TFDCNB

Temperature (K)	100.00(10)
Crystal System	triclinic
Space group	P-1
a/ Å	6.7353(3)
b/Å	11.3696(5)
c/Å	16.8733(8)
α/°	70.393(4)
β/°	86.036(4)
γ/°	79.883(4)
V/ Å^3	1198.20(10)
D_c/ g cm^{-3}	1.329
μ /mm^{-1}	0.842
$F(000)$	500
θ range/°	2.780-68.214
Reflections collected	10240
Unique reflections	4280
reflections I > 2σ(I)	3567
R_{int}	0.0420
Goodness of fit (F^2)	1.034
R1 ($I > 2σ(I)$)	0.0493
wR2($I > 2σ(I)$)	0.1331
CCDC No.	2260512

Py-TFDCNB

Temperature (K)	99.97(12)
Crystal System	monoclinic
Space group	$P2_1/c$
a/ Å	14.0212(3)
b/Å	8.3368(2)
c/Å	15.4457(4)
α/°	90
β/°	100.715(2)
γ/°	90
V/ Å^3	1774.00(7)
D_c/ g cm^{-3}	1.506
μ /mm^{-1}	1.015
$F(000)$	816
θ range/°	3.208-68.076
Reflections collected	16874
Unique reflections	3194
reflections I > 2σ(I)	2821
R_{int}	0.0465
Goodness of fit (F^2)	1.086
R1 ($I > 2σ(I)$)	0.0557

$wR2(I > 2\sigma(I))$	0.1459
CCDC No.	2260513

ETC-TCNB

Temperature (K)	293(2)
Crystal System	monoclinic
Space group	$C2/c$
a/ Å	14.2576(2)
b/Å	29.1258(4)
c/Å	9.46920(10)
α/°	90
β/°	93.6360(10)
γ/°	90
V/ Å^3	3924.30(9)
D_c/ g cm^{-3}	1.264
μ /mm^{-1}	0.618
$F(000)$	1552
θ range/°	3.035-68.194
Reflections collected	9209
Unique reflections	3541
reflections I > 2σ(I)	2953
R_{int}	0.0162
Goodness of fit (F^2)	1.043
$R1$ ($I > 2\sigma(I)$)	0.0489
$wR2(I > 2\sigma(I))$	0.1420
CCDC No.	2260514

References:

1. CrysAlisPRO. Agilent Technologies Ltd, Begbroke, Oxfordshire, England, Agilent (2014).

2. Sheldrick, G. M. SHELXT – Integrated Space-Group and Crystal-Structure Determination. ActaCrystallogr. A 2015, **71**, 3–8.

3. a) Oliver, W.C.; Pharr, G.M. Measurement of Hardness and Elastic Modulus by Instrumented Indentation: Advances in Understanding and Refinements to Methodology. J. Mater. Res. 2004, 19, 3–20; b) Oliver W.C.; Pharr, G.M. An Improved Technique for Determining Hardness and Elastic Modulus Using Load and Displacement Sensing Indentation Experiments. *J. Mater. Res.* 1992, **7**, 1564–1583.

4. M. K. Etherington, F. Franchello, J. Gibson, T. Northey, J. Santos, J. S. Ward, H. F. Higginbotham, P. Data, A. Kurowska, P. L. Dos Santos, D. R. Graves, A. S. Batsanov, F. B. Dias, M. R. Bryce, T. J. Penfold and A. P. Monkman, *Nat. Commun.*, 2017, **8**, 14987.

5. L. Yang, Y. Zhang, X. Zou, H. Lu, G. Li, *Green Chemistry* **2018**, *20*, 1362-1366.

6. G. R. Fulmer, A. J. M. Miller, N. H. Sherden, H. E. Gottlieb, A. Nudelman, B. M. Stoltz, J. E. Bercaw, K. I. Goldberg, *Organometallics* **2010**, *29*, 2176-2179.

7. Gaussian 16, Revision B.01, M. J. Frisch, G. W. Trucks, H. B. Schlegel, G. E. Scuseria, M. A. Robb, J. R. Cheeseman, G. Scalmani, V. Barone, G. A. Petersson, H. Nakatsuji, X. Li, M. Caricato, A. V. Marenich, J. Bloino, B. G. Janesko, R. Gomperts, B. Mennucci, H. P. Hratchian, J. V. Ortiz, A. F. Izmaylov, J. L. Sonnenberg, D. Williams-Young, F. Ding, F. Lipparini, F. Egidi, J. Goings, B. Peng, A. Petrone, T. Henderson, D. Ranasinghe, V. G. Zakrzewski, J. Gao, N. Rega, G. Zheng, W. Liang, M. Hada, M. Ehara, K. Toyota, R. Fukuda, J. Hasegawa, M. Ishida, T. Nakajima, Y. Honda, O. Kitao, H. Nakai, T. Vreven, K. Throssell, J. A. Montgomery, Jr., J. E. Peralta, F. Ogliaro, M. J. Bearpark, J. J. Heyd, E. N. Brothers, K. N. Kudin, V. N. Staroverov, T. A. Keith, R. Kobayashi, J. Normand, K. Raghavachari, A. P. Rendell, J. C. Burant, S. S. Iyengar, J. Tomasi, M. Cossi, J. M. Millam, M. Klene, C. Adamo, R. Cammi, J. W. Ochterski, R. L. Martin, K. Morokuma, O. Farkas, J. B. Foresman, and D. J. Fox, Gaussian, Inc., Wallingford CT, 2016.

8. M. A. Spackman and D. Jayatilaka, *CrystEngComm*, 2009, **11**, 19-32.

9. Turner, M. J., McKinnon, J. J., Wolff, S. K., Grimwood, D. J., Spackman, P. R., Jayatilaka, D. & Spackman, M. A. CrystalExplorer17 (2017). University of Western Australia. http://hirshfeldsurface.net